Inverse Problems and Imaging
Volume 11, No. 5, 2017, 783–798
doi:10.3934/ipi.2017037

A WAVELET FRAME APPROACH FOR REMOVAL OF MIXED GAUSSIAN AND IMPULSE NOISE ON SURFACES

Jianbin Yang* and Cong Wang
College of Science, Hohai University
No.8 Focheng West Road, Jiangning, Nanjing, Jiangsu Province, China, 211100

(Communicated by Hui Ji)

Abstract. Surface denoising is a fundamental problem in geometry processing and computer graphics. In this paper, we propose a wavelet frame based variational model to restore surfaces which are corrupted by mixed Gaussian and impulse noise, under the assumption that the region corrupted by impulse noise is unknown. The model contains a universal $\ell_1+\ell_2$ fidelity term and an ℓ_1-regularized term which makes additional use of the wavelet frame transform on surfaces in order to preserve key features such as sharp edges and corners. We then apply the augmented Lagrangian and accelerated proximal gradient methods to solve this model. In the end, we demonstrate the efficacy of our approach with numerical experiments both on surfaces and functions defined on surfaces. The experimental results show that our method is competitive relative to some existing denoising methods.

1. **Introduction.** Triangulated surface models are widely used in many fields such as computer graphics, reverse engineering, architectural design and terrain modelling. Compared with other surfaces, such as parametric and implicit surfaces, mesh surfaces are quite easy to obtain and operate. Additionally, they can approximate surfaces with arbitrary topology and geometry [2]. Such surfaces are usually acquired by 3D measurement technologies such as digital scanning devices which produce depth maps and ship-based sonar. Due to physical scanning processes and algorithm errors, measured mesh surface models often contain kinds of noise [24]. The noise may severely affect the usability of mesh models, and it is often desirable to remove noise to obtain high-quality surfaces before further processing. The main challenge in this task is to reduce noise and artifacts from an observed mesh surface, while preserving key features such as sharp edges and corners.

The mathematical model for mesh surface denoising can be stated as follows. We denote a triangular mesh by $\mathcal{M}=(\mathcal{V},\mathcal{E},\mathcal{F})$, where $\mathcal{V}=\{V(1),\cdots,V(n)\}$ is the vertex set, $\mathcal{E}=\{E(1),\cdots,E(e)\}$, $E(i)\in\mathcal{V}\times\mathcal{V}$ is the edge set, and $\mathcal{F}=\{F(1),\cdots,F(f)\},F(i)\in\mathcal{V}\times\mathcal{V}\times\mathcal{V}$ is the triangular face set. Here, let $V(i)=(V_1(i),V_2(i),V_3(i))^T$ be the (x,y,z)-coordinates of the vertex $V(i)$. We are interested in computation of a piecewise smooth function $S:\mathcal{M}\to\mathbb{R}^d$ on a triangle mesh. The function S can flexibly be chosen to describe vertex positions, texture

2010 *Mathematics Subject Classification.* Primary: 68U10, 47A52, 65T60; Secondary: 65K10.
Key words and phrases. Wavelet frame, surface denoising, mixed Gaussian and impulse noise, ALM-APG algorithm, variational model.
The first author is supported by NSF grant #11101120 and the Fundamental Research Funds for the Central Universities 2015B19514, China; The second author is supported by the Fundamental Research Funds for the Central Universities 2015B38014.
* Corresponding author: Jianbin Yang.

coordinates, vertex displacements, etc. For a discretization on the triangle mesh, we formulate S by the vector of sample values at the n mesh vertices

$$S : \mathcal{M} \to [S(V(1)), \cdots, S(V(n))]. \tag{1}$$

Let $\widetilde{S}(V(i)) = S(V(i)) + \epsilon_i N_i$ be the observed noisy surface where ϵ_i is a random variable and $N_i := N(V(i)) \in \mathbb{R}^3$ is the normal of the mesh for each vertex $V(i)$. The task of surface denoising is to approximate the true underlying surface S from $\widetilde{S}$.

Surface denoising is a fundamental problem in geometry processing and many attempts have been made in the past decade. Based on nonlinear diffusion equations and the theory of geometric evolution problems, some successful models used for image restoration have been extended to denoising surfaces (see e.g. [5, 6, 7, 11, 16, 27, 28] and the references therein). For instance, in [6] an important geometric model for surface denoising was proposed using diffusion and curvature flow. Moreover, authors in [11] established a variational model analogous to the ROF model [23] in the context of geometry processing. Recently, based on the sparsity of the gradient of the face normal field, a variational model in [31] was proposed for mesh denoising. Other approaches for surface denoising include the classical Laplacian smoothing method [2], bilateral filtering [13, 17], normal filtering and vertex updating [26]. More recently, based on a tight wavelet frame representation of surfaces, an analysis based surface denoising model was proposed in [9].

When the perturbation in (1) is additive white Gaussian noise, i.e. $\epsilon_i \sim \mathcal{N}(0, \sigma^2)$, it is mostly considered in the above literature for its good characterization of system noise. However, non-Gaussian type noise are also encountered in many real observations due to noisy sensors and channel transmission [15, 24]. Moreover, although in image processing, a vast amount of literature is devoted to non-Gaussian noise problems, such as impulse noise, Poisson noise and mixed Poisson-Gaussian noise (see [15, 18, 25, 29] and many references therein), there are few studies in surface denoising with non-Gaussian noise.

In this paper we study how to effectively remove mixed Gaussian and impulse noise in surface functions. These noises are caused by errors in data transmission or faulty memory location in hardware. We assume that either additive Gaussian white noise or impulse noise takes the form of randomly occurring displacement of the vertices along the normal direction. Mathematically speaking, let $\widetilde{S}$ be an observed corrupted surface, i.e.

$$\widetilde{S}(V(i)) = \begin{cases} S(V(i)) + \epsilon_1 N(V(i)) & V(i) \in \mathcal{V}_1 \\ \epsilon_2 N(V(i)) & V(i) \in \mathcal{V}_2 := \mathcal{V} \backslash \mathcal{V}_1 \end{cases}, \tag{2}$$

where $\mathcal{V}_1$ is unknown, $\epsilon_1 N(V(i))$, $V(i) \in \mathcal{V}_1$ denotes the independent identically distributed (i.i.d.) additive Gaussian noise, and $\epsilon_2 N(V(i))$, $V(i) \in \mathcal{V}_2$ denotes the i.i.d. random-valued impulse noise. The subset $\mathcal{V}_2$ denotes the region where the information of S is missing. It is assumed to be unknown with each element being drawn from the whole region $\mathcal{V} = \{V(i), \cdots, V(n)\}$ by Bernoulli trial with a given probability $0 \leq p \leq 1$.

We denote $r := |\mathcal{V}_2|/|\mathcal{V}|$ as the level of impulse noise. If $\mathcal{V}_2$ is empty, there is no impulse noise, then the problem in (2) becomes the surface denoising problem for removing Gaussian noise. If the region $\mathcal{V}_2$ is known in advance, this can be considered as a mesh repair problem. If $\mathcal{V}_2$ is a proper subset of $\mathcal{V}$, the observation $\widetilde{S}$ of a surface function S is said to be corrupted by the mixed Gaussian and impulse

noise. Under the assumption that the region $\mathcal{V}_2$ is unknown in advance, the goal of this paper is to approximate S from the observed surface function $\widetilde{S}$.

The challenge of this problem is to preserve key features of surface functions such as sharp edges and corners, while removing noise and spurious information simultaneously. For image processing problems, the variational model

$$\min_{u\in\mathbb{R}^{m\times n}} F(u)+\lambda\Gamma(u) \tag{3}$$

has been successfully applied to image denoising, inpainting, deconvolution, etc (see e.g. [3, 4, 10, 15, 18, 23, 29, 30]). Here, $F(u)$ is a fidelity term which keeps the image u close enough to the observed image, $\Gamma(u)$ is a regularization term for modeling a priori knowledge on unknown images, and λ is a positive parameter balancing the two terms. The fidelity term $F(u)$ takes different forms according to different noise statistics and is designed based on the noise characteristic. For example, it is well known that the least square fidelity is used for additive white Gaussian noise. Less well known is the Kullback-Leibler (KL)-divergence fidelity for Poisson noise and ℓ_1-norm fidelity for impulse noise [15, 18]. The regularization term $\Gamma(u)$ is designed based on a priori assumption on original image. One of the assumptions commonly used is the sparsity of the underlying solution in some transformed domain. Such transforms can be discrete gradient used in total variation [23], wavelet tight frame transform [3, 4, 10, 18], local cosine transforms, etc.

We here extend the idea of (3) to surface denoising. To remove mixed Gaussian and impulse noise on surfaces, we choose the fidelity term $F(S) = \|S-\widetilde{S}\|_{\ell_1}+\frac{\lambda}{2}\|S-\widetilde{S}\|^2_{\ell_2}$, where $\|S-\widetilde{S}\|_{\ell_1} := \sum_{i=1}^n |S(V(i))-\widetilde{S}(V(i))|$, $\|S-\widetilde{S}\|^2_{\ell_2} := \sum_{i=1}^n |S(V(i))-\widetilde{S}(V(i))|^2$, and λ is a parameter. This fidelity term was first introduced in [15] for image restoration with mixed or unknown noises. We choose the regularization term $\Gamma(S) = \|\mathcal{W}S\|_{\ell_1} := \sum_{i=1}^n |\mathcal{W}S(V(i))|$, where $\mathcal{W}$ is the discrete wavelet frame transform on surfaces, see Section 2.1 for details. The basic idea behind the regularization term is to make use of the interaction between the wavelet frame transform and the ℓ_1-norm. It is well known that the wavelet coefficient sequence of a signal, which is sampled from a piecewise smooth function, is sparse. Furthermore, because of the ℓ_1-norm, the regularization term $\|\mathcal{W}S\|_{\ell_1}$ gives preference to a solution S whose wavelet coefficient sequence is sparse, and to keep the edges and corners of surface functions. The extension of image restoration model to surface denoising is not trivial because of the nonlinear nature of the surfaces and the corresponding algorithm [9, 31].

Combining the fidelity term and the regularization term together, we have the following wavelet frame based model

$$\min E(S) := \|S-\widetilde{S}\|_{\ell_1}+\frac{\lambda}{2}\|S-\widetilde{S}\|^2_{\ell_2}+\nu\|\mathcal{W}S\|_{\ell_1} \tag{4}$$

for removal of mixed noise on surfaces. The model (4) is an ordinary least squares problem with an ℓ_1-fidelity term and an ℓ_1-regularization term. It means that this problem cannot be solved straight forward by solving only one system of equations. However, if we write the two ℓ_1-terms in a matrix form, (4) becomes a least squares problem with an ℓ_1-fidelity term. Then, iterative solvers like the augmented Lagrangian method (ALM) can be applied to solve (4).

The rest of this paper is organized as follows. In Section 2.1 we introduce the wavelet frame transform on surfaces. In Section 2.2 we derive a wavelet frame based model and the corresponding algorithm to remove the mixed noise on surfaces. In

Section 3 we present some numerical examples and discussions. In the last section we give a conclusion.

2. Mathematical modeling and algorithm.

2.1. **Wavelet frame transform on surfaces.** Before presenting our proposed regularization for surface denoising, we briefly review a few facts of discrete tight wavelet frame decomposition and reconstruction. The interesting readers should consult [9, 10, 19] for a more detailed survey. Note that in the discrete setting, an image is a 2D array that can be understood as a vector living on a discrete grid. Then the discrete wavelet tight frame decomposition can be represented as a matrix multiplication $\mathcal{W}$, where $\mathcal{W}$ is derived by all the refinement masks (filters) of a wavelet tight frame system. Correspondingly, by the unitary extension principle [22], the reconstruction operator $\mathcal{W}^T$ can be defined similarly by the transpose of refinement masks and we have $\mathcal{W}^T\mathcal{W} = \mathcal{I}$. In the implementation, these two matrix multiplications are done by using the fast tensor product tight wavelet frame decomposition and reconstruction algorithms instead, which are essentially just the convolution of images by a set of filters.

However, due to the difference of topological structures between surface and image, we can not directly apply wavelet frame transform in image processing to surface denoising. Recently, motivated by the works in [12] which construct non-tensor-product tight wavelet frames by dual Gramian analysis on Hilbert spaces, Dong et al. in [9] introduced a multiscale representation of surfaces using a data matrix and a corresponding wavelet frame matrix. For the triangular mesh $\mathcal{M} = (\mathcal{V}, \mathcal{E}, \mathcal{F})$, let the vertex set $\mathcal{V} := \{V(k),\ k = 1, 2, \cdots, n\}$, where $V(k) = (V_1(k), V_2(k), V_3(k))^T$ is the (x, y, z)-coordinates of the vertex $V(k)$. For each $k \in \{1, 2, \cdots, n\}$, if $V(k) \in \mathcal{V}$ has degree 6, we find the six neighboring vertices of $V(k)$ and denoted as $\{P(k, 1), P(k, 2), \cdots, P(k, 6)\}$, see FIGURE 1. Then for a function S defined on the triangle mesh,

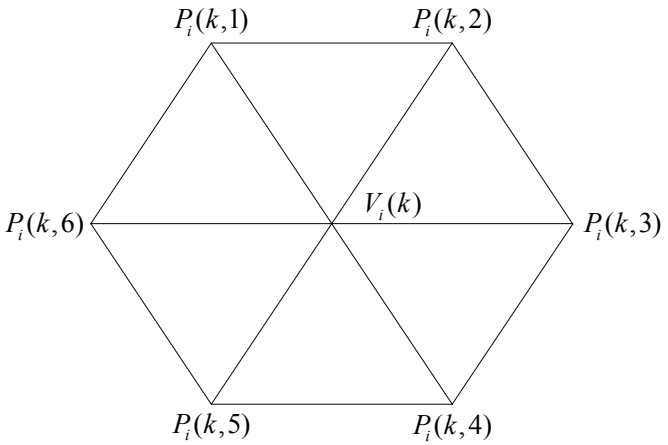

FIGURE 1. This figure illustrates how the neighboring vertices of a given vertex $V_i(k)$ are ordered.

a data matrix F_i, $i = 1, 2, 3$, consisting of the set of neighboring function values is a matrix in $\mathbb{R}^{7\times n}$ defined by

$$F_i = \begin{bmatrix} S(V_i(1)) & \cdots & S(V_i(k)) & \cdots & S(V_i(n)) \\ S(P_i(1,1)) & \cdots & S(P_i(k,1)) & \cdots & S(P_i(n,1)) \\ S(P_i(1,2)) & \cdots & S(P_i(k,2)) & \cdots & S(P_i(n,2)) \\ S(P_i(1,3)) & \cdots & S(P_i(k,3)) & \cdots & S(P_i(n,3)) \\ S(P_i(1,4)) & \cdots & S(P_i(k,4)) & \cdots & S(P_i(n,4)) \\ S(P_i(1,5)) & \cdots & S(P_i(k,5)) & \cdots & S(P_i(n,5)) \\ S(P_i(1,6)) & \cdots & S(P_i(k,6)) & \cdots & S(P_i(n,6)) \end{bmatrix},$$

where $(P_1(k,j), P_2(k,j), P_3(k,j))^T$, $j = 1, 2, \cdots, 6$, is the (x, y, z)-coordinates of $P(k,j)$. We let $F := \{F_1, F_2, F_3\}$. Finally, if the degree d of some vertex is not 6, we can generate 6 neighboring values $S(P_i(k,j))$ with average values of the d neighboring values. Let $\widehat{S}(P_i(k,t)), t = 1, \ldots, d$ be the d neighboring values. Then, we set $S(P_i(k,j)) = \frac{1}{6}\sum_{t=1}^{d} \widehat{S}(P_i(k,t))$, $j = 1, 2, \cdots, 6$.

Following [9], we define a mask matrix M in $\mathbb{R}^{7\times 7}$ as

$$M = \frac{1}{8}\begin{bmatrix} 2 & 1 & 1 & 1 & 1 & 1 & 1 \\ 2 & -1 & -1 & 1 & -1 & -1 & 1 \\ 2 & 1 & -1 & -1 & 1 & -1 & -1 \\ 2 & -1 & 1 & -1 & -1 & 1 & -1 \\ 0 & -\frac{2\sqrt{3}}{3} & -\frac{2\sqrt{3}}{3} & -\frac{2\sqrt{3}}{3} & \frac{2\sqrt{3}}{3} & \frac{2\sqrt{3}}{3} & \frac{2\sqrt{3}}{3} \\ 0 & \frac{\sqrt{6}}{3} & \frac{\sqrt{6}}{3} & -\frac{2\sqrt{6}}{3} & -\frac{\sqrt{6}}{3} & -\frac{\sqrt{6}}{3} & \frac{2\sqrt{6}}{3} \\ 0 & \sqrt{2} & -\sqrt{2} & 0 & -\sqrt{2} & \sqrt{2} & 0 \end{bmatrix}.$$

Here, the first row of M is a low-pass filter and $2-7th$ row of M are high-pass filters. This set of filters (refinement masks) of tight wavelet frames was constructed in [12] by linear bivariate box spline with directions $(1,0)^T$, $(0,1)^T$ and $(1,1)^T$.

Noting that the order of the coefficients of each filter in M is harmonious with the neighborhood of the vertex $V(k)$ which forms the column of the data-matrix. We define the (1-level) wavelet frame decomposition on a mesh surface as

$$\mathcal{W}S := MF = \{MF_1, MF_2, MF_3\} = \alpha, \tag{5}$$

where $\alpha := \{\alpha_1, \alpha_2, \alpha_3\}$ with matrix $\alpha_i = MF_i$. Similarly, the reconstruction operator $\mathcal{R}$ can be defined as

$$\mathcal{R}\alpha = \delta_0 M^{-1}\alpha,$$

where $\delta_0 := [1,0,0,0,0,0,0]$. It is easy to check that the vector $\mathbf{r} := [1,1,1,1,0,0,0]$ is the first row of M^{-1} and

$$\mathbf{r}M = \delta_0 = [1,0,0,0,0,0,0].$$

Then, for numerical simplicity, we define $\mathcal{R}$ as

$$\mathcal{R}(\alpha) = \mathbf{r}(\alpha) = \{\mathbf{r}(\alpha_1), \mathbf{r}(\alpha_2), \mathbf{r}(\alpha_3)\}.$$

Thus, we have $\mathcal{R}\mathcal{W}S = S$. We omit discussions on high-level wavelet frame transform on surfaces here and the interested reader is referred to [8, 9] for details.

2.2. **Model and algorithm.** For a given triangular mesh $\mathcal{M}$ and a noisy function $\widetilde{S}$ defined on $\mathcal{M}$, our task is to remove the mixed Gaussian and impulse noise from $\widetilde{S}$. Here, the function $\widetilde{S}$ can be chosen to describe vertex positions, vertex displacements, a piecewise smooth function on a two dimensional smooth manifold, etc. Motivated by the impressive performance of wavelet frame image restoration methods (see e.g. [3, 4, 10, 18, 19, 25, 30]), we also use the wavelet frame coefficients

to build a new characterization of functions on mesh surfaces with key features. To remove the mixed noise from $\widetilde{S}$, we consider the following variational model

$$\min_S \|S-\widetilde{S}\|_{\ell_1}+\frac{\lambda}{2}\|S-\widetilde{S}\|_{\ell_2}^2+\nu\|\mathcal{W}S\|_{\ell_1}, \tag{6}$$

where λ and ν are two positive parameters and $\mathcal{W}$ is the wavelet frame transform on surfaces. The first two terms of (6) are the fitting terms with

$$\|S-\widetilde{S}\|_{\ell_1}:=\sum_{i=1}^{3}\sum_{j=1}^{n}|S(V_i(j))-\widetilde{S}(V_i(j))|$$

and

$$\|S-\widetilde{S}\|_{\ell_2}^2:=\sum_{i=1}^{3}\sum_{j=1}^{n}|S(V_i(j))-\widetilde{S}(V_i(j))|^2.$$

The last term of (6) is a regularization term with

$$\|\mathcal{W}S\|_{\ell_1}:=\|\alpha\|_{\ell_1}=\sum_{i=1}^{3}\sum_{j=1}^{n}(\sum_{\ell=2}^{7}|\alpha_i[\ell,j]|^2)^{\frac{1}{2}},$$

which was defined by (5).

Since the optimization model (6) is a least squares problem with an ℓ_1-fitting term and an ℓ_1-regularization term, this problem cannot be solved straight forward by solving only one system of equations. To apply certain fast iterative solvers for this ℓ_1/ℓ_2-problem, we first replace (6) with the following matrix form:

$$\min_S \frac{\lambda}{2}\|S-\widetilde{S}\|_{\ell_2}^2+\beta^T|AS-C|, \tag{7}$$

where

$$A:=\begin{pmatrix} I \\ \mathcal{W}\end{pmatrix},\quad C:=\begin{pmatrix}\widetilde{S}\\ 0\end{pmatrix},\quad \beta:=\begin{pmatrix} e\\ \nu\widehat{e}\end{pmatrix},$$

I is an identity matrix, e and $\widehat{e}$ are vectors of ones, and $|\cdot|$ denotes a column vector of absolute values. Next, we reformulate (7) by introducing a new variable Z:

$$\min_{S,Z} f(S,Z):=\frac{\lambda}{2}\|S-\widetilde{S}\|_{\ell_2}^2+\beta^T|Z|,\quad \text{s.t. } AS-C+Z=0. \tag{8}$$

In the following, we apply the augmented Lagrangian method (ALM) [21] to solve (8). First, let us define the augmented Lagrangian function of (8) associated with a given parameter $\sigma>0$:

$$\begin{aligned}\mathcal{L}_\sigma(S,Z;y):&=f(S,Z)+\langle y,C-AS-Z\rangle+\frac{\sigma}{2}\|C-AS-Z\|_{\ell_2}^2\\ &=f(S,Z)+\frac{\sigma}{2}\|C-AS-Z+\frac{1}{\sigma}y\|_{\ell_2}^2-\frac{1}{2\sigma}\|y\|_{\ell_2}^2.\end{aligned}$$

Then, the ALM for solving (8) is summarized as follows:

Here, we choose the calculation error $\varepsilon=10^{-4}$. The main task of ALM iteration is to solve the inner subproblem

$$\begin{aligned}&\min_{S,Z}\mathcal{L}_{\sigma_k}(S,Z;y^k)\\ =&\min_{S,Z}\frac{\lambda}{2}\|S-\widetilde{S}\|_{\ell_2}^2+\beta^T|Z|+\frac{\sigma_k}{2}\|C-AS-Z+\frac{1}{\sigma_k}y^k\|_{\ell_2}^2-\frac{1}{2\sigma_k}\|y^k\|_{\ell_2}^2.\end{aligned} \tag{9}$$

Algorithm 1 ALM Algorithm

Initialize: Given a tolerance $\varepsilon > 0$. Input y^0, y^{-1} and $\sigma_0 > 0$. $k = 0$.
while $\|(y^k - y^{k-1})/\sigma_k\| \geq \varepsilon$ **do**
$(S^{k+1}, Z^{k+1}) = \arg\min_{S,Z} \mathcal{L}_{\sigma_k}(S, Z; y^k)$
$y^{k+1} = y^k + \sigma_k(C - AS^{k+1} - Z^{k+1})$
$\sigma_{k+1} = \sigma_k + 1$
$k = k + 1$
end while

First, for fixed S, we consider the minimization of $\mathcal{L}_{\sigma_k}(S, Z; y^k)$ in terms of Z. Let

$$\eta := \sigma_k(C - AS) + y^k.$$

Then, the minimization of $\mathcal{L}_{\sigma_k}(S, Z; y^k)$ is equivalent to

$$\min_Z \frac{1}{\sigma_k}\beta^T|Z| + \frac{1}{2}\|Z - \frac{\eta}{\sigma_k}\|_{\ell_2}^2,$$

which has a closed form solution given by:

$$Z = \frac{1}{\sigma_k}\mathcal{T}_\beta(\eta). \tag{10}$$

Here, for $\beta > 0$, $\mathcal{T}_\beta$ is the soft-threshold operator

$$\mathcal{T}_\beta(\eta) := [t_{\beta_1}(\eta_1), t_{\beta_2}(\eta_2), \ldots, t_{\beta_M}(\eta_M)]^T,$$

with $t_{\beta_i}(\eta_i) := \operatorname{sgn}(\eta_i) \cdot \max\{|\eta_i| - \beta_i, 0\}$. Note that $\mathcal{T}_\beta(\eta)$ is composed of two parts: one is thresholding on the surface function values, $\mathcal{T}_e(\sigma_k(\tilde{S} - S) + y_1^k)$; the other is thresholding on the wavelet frame coefficients, $\mathcal{T}_{\nu\hat{e}}(\sigma_k(\mathcal{W}S) + y_2^k)$. Here, $y^k := (y_1^k, y_2^k)^T$.

Substitute (10) into (9), one can check that

$$\min_Z \beta^T|Z| + \frac{\sigma_k}{2}\|C - AS - Z + \frac{1}{\sigma_k}y^k\|_{\ell_2}^2 = \frac{1}{\sigma_k}\sum_i \phi_{\beta_i}(\eta_i), \tag{11}$$

where $\phi_\varepsilon(t)$ is the Huber function defined by

$$\phi_\varepsilon(t) := \begin{cases} \frac{1}{2}t^2 & |t| \leq \varepsilon \\ \varepsilon|t| - \frac{1}{2}\varepsilon^2 & |t| > \varepsilon \end{cases},$$

$\eta = (\eta_1, \eta_2, \ldots)^T$ and $\beta = (\beta_1, \beta_2, \ldots)^T$.

Therefore, to solve the subproblem (9), we need to find the optimal S of the following unconstrained convex optimization problem

$$\min_S H(S) := \frac{1}{\sigma_k}\sum_i \phi_{\beta_i}(\eta_i) + \frac{\lambda}{2}\|S - \widetilde{S}\|_{\ell_2}^2. \tag{12}$$

Following [14], we apply the accelerated proximal gradient (APG) method [10, 20] to solve (12), where the gradient of H is given by

$$\nabla H(S) = -A^T(\eta - \mathcal{T}_\beta(\eta)) + \lambda(S - \widetilde{S}).$$

Note that A has full column rank and $H(S)$ is a strictly convex function. Hence, the above minimization has a unique solution.

The APG algorithm is summarized as follows:

Algorithm 2 APG Algorithm

Initialize: Given $S_0 = S_1 = \widetilde{S}, t_0 = t_1 = 1, \tau = 1$
for $i = 1$ to p **do**
$\bar{S}_i = S_i + \frac{t_{i-1}-1}{t_i}(S_i - S_{i-1})$
$S_{i+1} = \bar{S}_i - \tau \nabla H(\bar{S}_i)$
$t_{i+1} = \frac{1+\sqrt{1+4(t_i)^2}}{2}$
end for

Here, we choose the number of iterations $p = 25$, and the step length of APG algorithm $\tau = 1$. In conclusion, the ALM-APG algorithm for solving (6) is summarized in **Algorithm 3**.

Algorithm 3 ALM-APG Algorithm

Initialize: Given $\varepsilon > 0, S^0 = \widetilde{S}, y^0 = y^{-1} = \vec{0}, \tau = 1, \sigma_0 = 1, k = 0$
while $\|(y^k - y^{k-1})/\sigma_k\| \geq \varepsilon$ or $k = 0$ **do**
Let $S_0 = S_1 = S^k, t_0 = t_1 = 1$
for $i = 1$ to p **do**
$\bar{S}_i = S_i + \frac{t_{i-1}-1}{t_i}(S_i - S_{i-1})$
$S_{i+1} = \bar{S}_i - \tau \nabla H(\bar{S}_i)$
$t_{i+1} = \frac{1+\sqrt{1+4(t_i)^2}}{2}$
end for
Set $S^{k+1} = S_{p+1}$, $Z^{k+1} = \frac{1}{\sigma_k}\mathcal{T}_\beta(\sigma_k(C - AS^{k+1}) + y^k)$
$y^{k+1} = y^k + \sigma_k(C - AS^{k+1} - Z^{k+1})$
$\sigma_{k+1} = \sigma_k + 1$
$k = k + 1$
end while

3. **Numerical results and discussions.** In this section, we present numerical experiments and compare our method with certain existing methods to verify the effectiveness of our method. The synthetic data are generated by clean functions on meshes with additive Gaussian noise and impulse noise. The meshes are normalized before test. All the examples are tested on a laptop with Intel Core i3 and 6 GB RAM and all models are rendered using flat shading.

We provide three kinds of numerical experiments to test the performance of our method for suppressing Gaussian and impulse noise, and then compare its performance with recently proposed algorithm in [31] and other variational models. The methods are abbreviated as Zhang et al.'s method [31], ℓ_2-variational model, ℓ_1-variational model and our $(\ell_2 + \ell_1)$-variational model in the following. Denoising results of the algorithm in [31] are kindly provided to us by the authors.

There are two common types of impulse noise: salt-and-pepper impulse noise and random-valued impulse noise. Since a vertex coordinate contaminated by random-valued impulse noise is not as distinctively an outlier as that contaminated by the salt-and-pepper noise, it is more difficult to detect. Thus we only consider the

random-valued impulse noise, which is defined as follows: with probability r, the function value $S(V(i))$ on vertex $V(i)$ is altered to be an uniform random value in the interval between the minimum and maximum value of the surface. With probability $1-r$, the function value $S(V(i))$ on $V(i)$ is disturbed by additive Gaussian noise $\mathcal{N}(\mu, \sigma^2)$. The mixed noise level of following examples are given by three parameters r, μ and σ.

3.1. **Numerical examples.** In this subsection, we show the experimental processes and results on surface denoising of our method. In the first experiment, two noisy surfaces, named 'elephant' and 'bunny', are simulated by displacement of the vertices along the normal direction (see FIGURE 2). We first add mixed Gaussian and impulse noise to clean surfaces, then apply our approach to remove noise. Denoising results are illustrated in FIGURE 2.

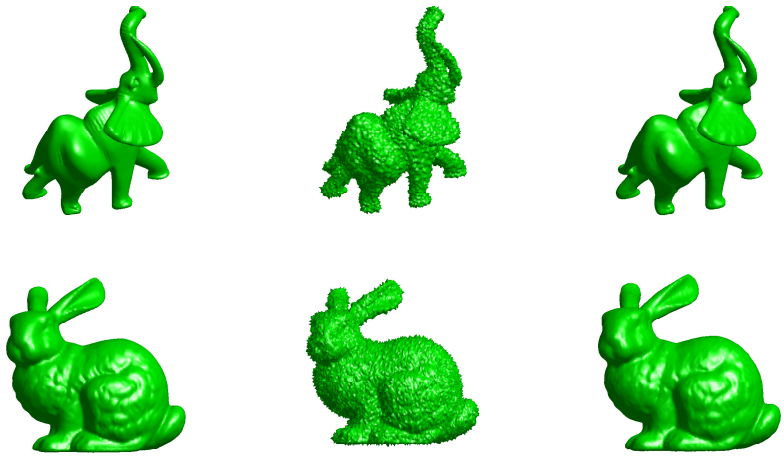

FIGURE 2. The elephant model (first row) and the bunny model (second row) are artificially corrupted by mixed Gaussian and impulse noise ($r = 20\%, \mu = 0, \sigma = 0.005$), then smoothed by our approach ($\lambda = 11, \nu = 0.2$). From left to right: noisy-free surfaces, noisy surfaces, denoising surfaces.

In the second experiment, we test the performance of surface function denoising. First, we choose manifold Ω_1 to be the unit sphere in $\mathbb{R}^3$ and define a function on Ω_1 as

$$S_1(x, y, z) := 1 + x^8 + e^{2y^3} + e^{2z^2} + 10xyz.$$

As in [1], we visualize this function as a kind of offset surface to the manifold, i.e., we consider the new surface as

$$\xi + S_1(\xi) N_\xi : \quad \xi \in \Omega_1,$$

where N_ξ denotes the unit outer normal to the manifold Ω_1 at ξ, see FIGURE 3. Similarly, we choose manifold Ω_2 to be the 'twelve' model and define function

$$S_2(x, y, z) := [1 \quad 0 \quad 0]^T.$$

Then, we obtain a new surface defined by

$$\xi + S_2(\xi) .* N_\xi : \quad \xi \in \Omega_2.$$

The new noisy-free surfaces are illustrated in the first column of FIGURE 3.

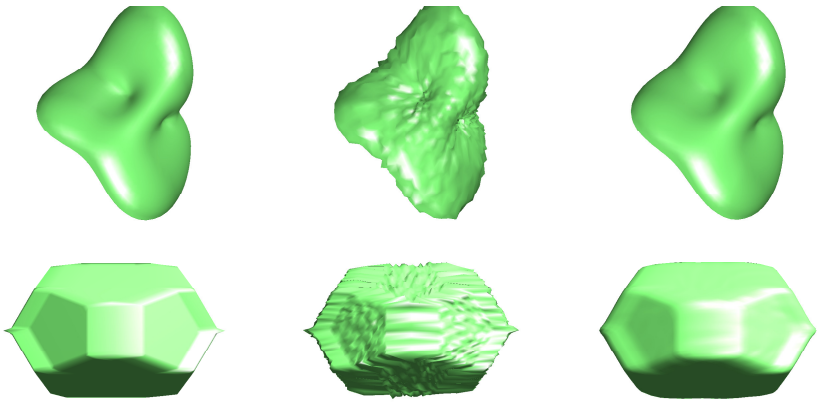

FIGURE 3. From left to right: noisy-free surfaces, noisy surfaces, denoising surfaces ($r = 40\%, \mu = 0, \sigma = 0.2, \lambda = 11, \nu = 0.2$).

In the last experiment, we consider a graph G, and the vertices set $\mathcal{V}$ of G are sampled from a unit sphere. The functions $f_G : \mathcal{V} \mapsto \mathbb{R}$ are generated by mapping two images, 'Slope' and 'Eric Cartman', onto the graph G (see FIGURE 4). Let the observed graph data be perturbed by the mixed noise along the normal direction. The denoising results are presented in FIGURE 5.

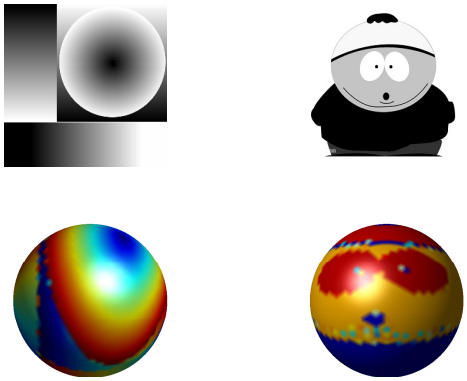

FIGURE 4. This figure shows two images (first row), 'Slope' and 'Eric Cartman', that are mapped to the graph of the unit sphere to form graph data f_G (second row).

3.2. **Comparisons to Zhang et al.'s method.** In this subsection, we present comparative results for removal of mixed Gaussian and impulse noise between Ours and Zhang et al.'s method [31]. It keeps consistent in all parameters of noise level between the two methods.

In FIGURE 6, we show the different performance between Ours and Zhang et al.'s method of the first experiment in Section 3.1. FIGURE 6 shows that our

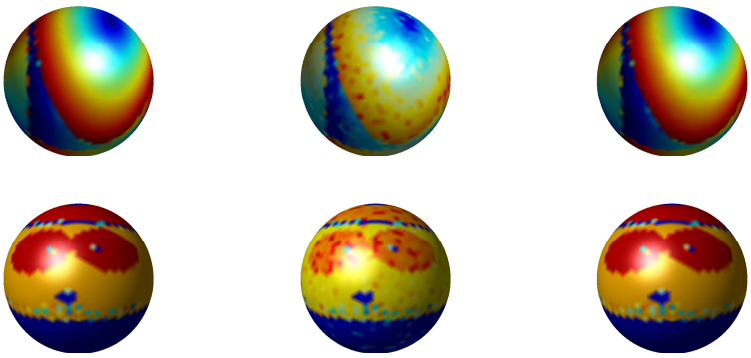

FIGURE 5. From left to right: noisy-free surfaces, noisy surfaces, denoising surfaces ($r = 20\%, \mu = 0, \sigma = 0.02, \lambda = 0.8, \nu = 0.035$).

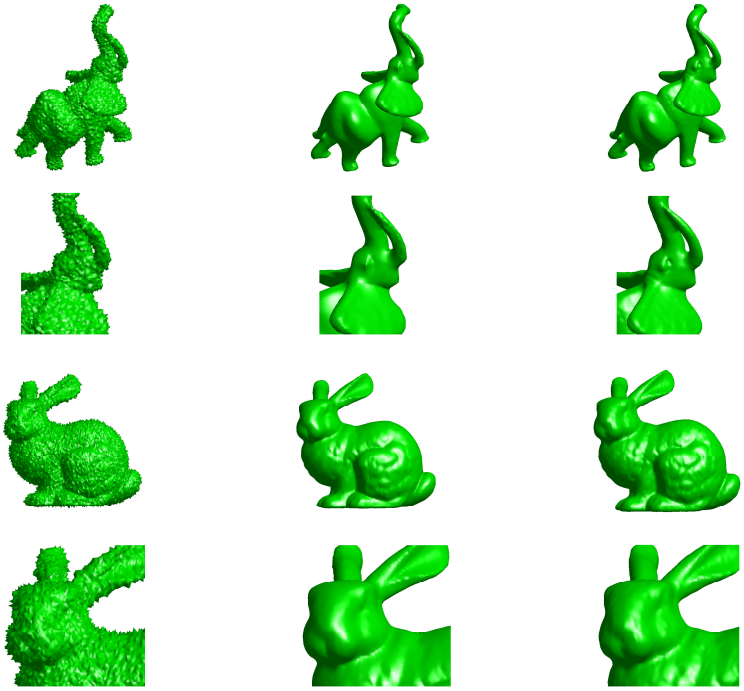

Noisy Zhang et al.'s results[31] Ours

FIGURE 6. From left to right: noisy surfaces, Zhang et al.'s results [31], Ours ($r = 20\%, \mu = 0, \sigma = 0.005$). The $2nd$ row and $4th$ row show zoomed view of surfaces.

method can preserve most sharp edges and corners better (see the zoomed view in FIGURE 6). In addition, we can also keep the shallow edge well.

In FIGURE 7, we present results and comparisons of the second experiment in Section 3.1. A zoomed view of the region indicates that Zhang et al.'s method

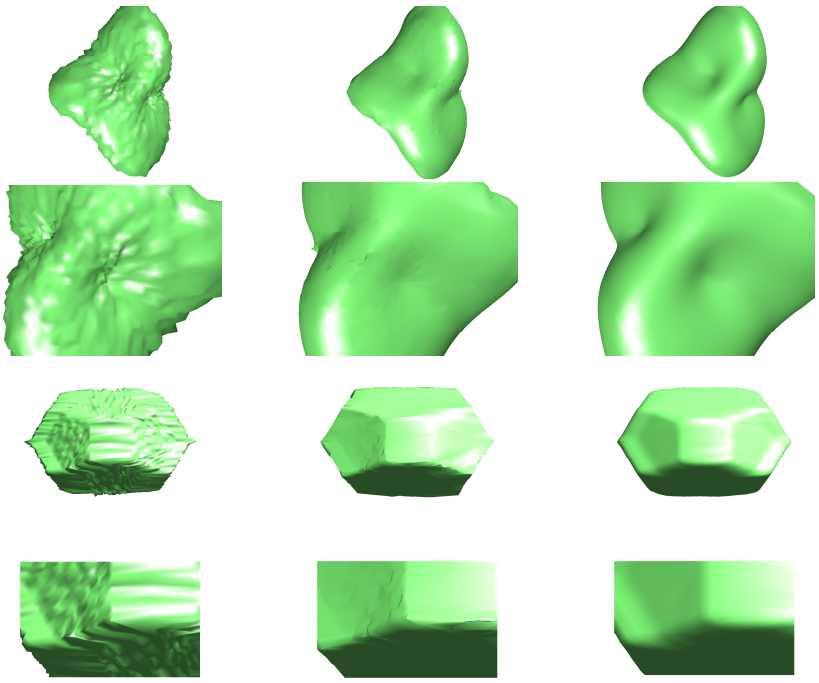

Noisy Zhang et al.'s results [31] Ours

FIGURE 7. It shows denoising results. From left to right: noisy surfaces, Zhang et al.'s results, Ours ($r = 40\%, \mu = 0, \sigma = 0.2$). The $2nd$ row and $4th$ row show zoomed view of surfaces.

generates false edges in smooth regions (see second column of FIGURE 7). In contrast, our method can keep features well.

TABLE 1. SNRs Comparison for removal of mixed Gaussian and impulse noise

Model	Zhang et al.'s	Ours
FIGURE 6 Row 1	43.735	45.035
FIGURE 6 Row 3	43.985	44.876
FIGURE 7 Row 1	42.833	45.565
FIGURE 7 Row 3	40.658	43.035

The quality of the denoised result $\overline{S}(V)$ can also be measured in terms of signal-to-noise ratio (SNR), which is defined by

$$\mathrm{SNR}(\overline{S}(V), S(V)) = -20 \log_{10} \frac{\|\overline{S}(V) - S(V)\|_{\ell_2}}{\|S(V)\|_{\ell_2}},$$

where $S(V)$ denotes the noisy-free surface functions. For the examples shown in FIGURE 6 and FIGURE 7, SNRs are computed and listed in TABLE 1. In conclusion, visual and quantitative comparisons illustrate the better performance of our method.

3.3. **Comparisons to other variational models.** In order to highlight the effectiveness of our model, we here compare our method with ℓ_2-variational model, i.e.

$$\min_S \frac{1}{2}\|S-\widetilde{S}\|_{\ell_2}^2+\nu\|\mathcal{W}S\|_{\ell_1}$$

and ℓ_1-variational model, i.e.

$$\min_S \|S-\widetilde{S}\|_{\ell_1}+\nu\|\mathcal{W}S\|_{\ell_1}.$$

Comparative results are listed in TABLE 2 and FIGURE 8-10.

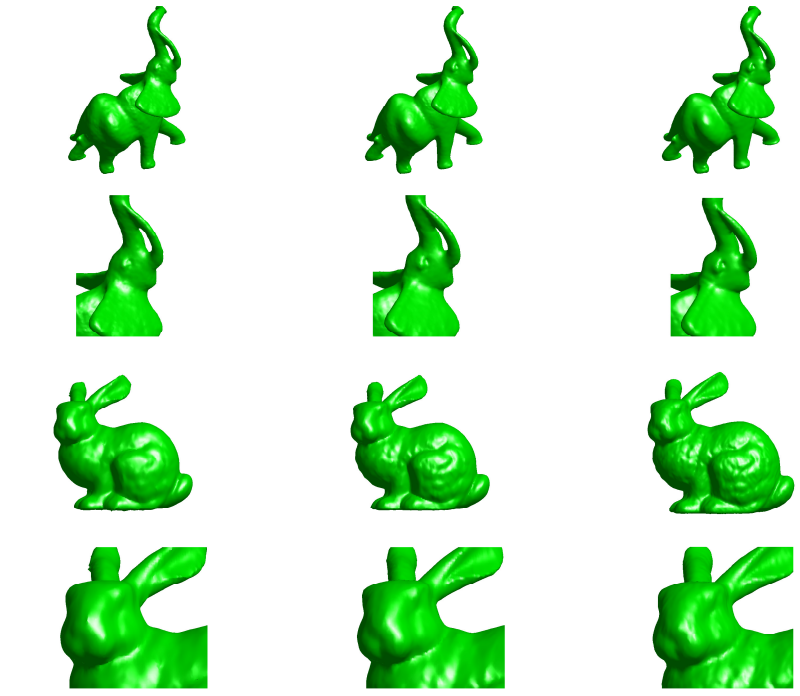

ℓ_2-variational model ℓ_1-variational model Ours

FIGURE 8. From left to right: results of ℓ_2-variational model, results of ℓ_1-variational model, Ours. The $2nd$ row and $4th$ row show zoomed view of surfaces.

TABLE 2. SNRs Comparison with other variational models

Model	ℓ_2-variational model	ℓ_1-variational model	Ours
elephant	42.858	43.064	45.035
bunny	43.027	43.356	44.876
Ω_1	42.024	42.410	45.565
Ω_2	40.674	40.787	43.035
Slope	28.688	29.647	31.231
Eric Cartman	29.063	29.953	31.087

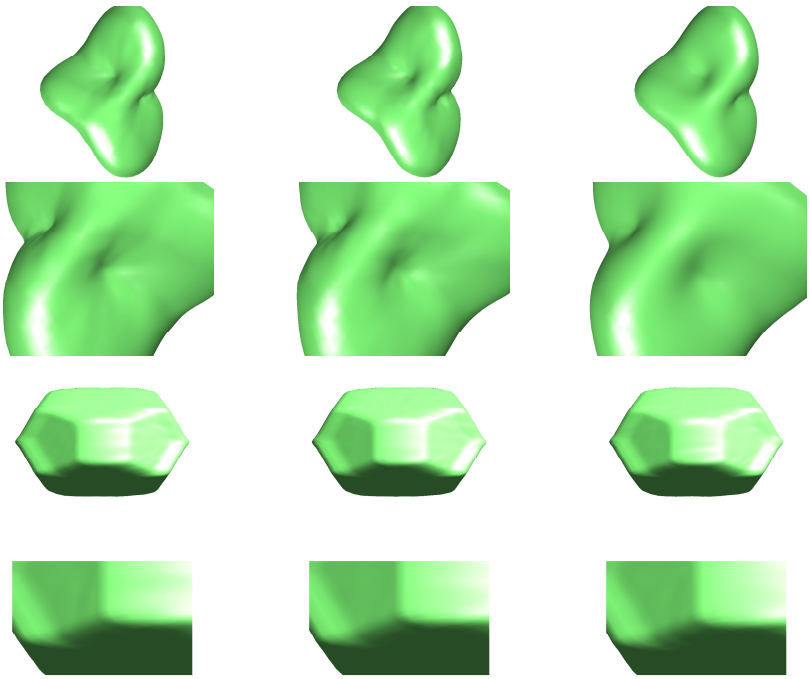

ℓ_2-variational model ℓ_1-variational model Ours

FIGURE 9. It shows denoising results. From left to right: results of ℓ_2-variational model, results of ℓ_1-variational model, Ours. The $2nd$ row and $4th$ row show zoomed view of surfaces.

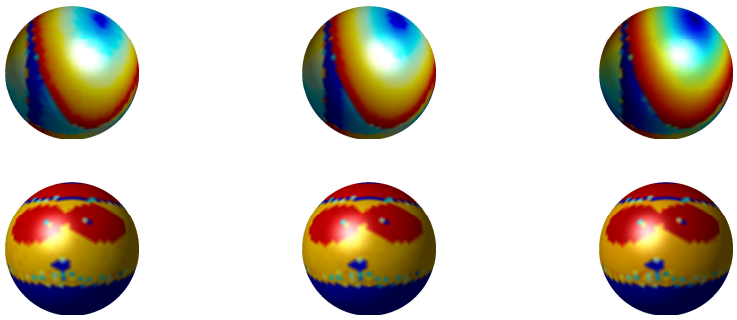

ℓ_2-variational model ℓ_1-variational model Ours

FIGURE 10. From left to right: results of ℓ_2-variational model, results of ℓ_1-variational model, Ours.

4. **Conclusion.** In this paper, we proposed a tight wavelet frame based model to simultaneously suppress mixed Gaussian and impulse noise on surfaces, under the assumption that the impulse noise region is unknown. We considered both surfaces and functions defined on surfaces. Based on topological structure of surfaces, we first

defined wavelet frame transform on surface functions. Then we applied the ALM-APG algorithm to solve the proposed model. In addition, we implemented three kinds of experiments to verify the practicability and effectiveness of our method. In the end, we compare our approach with Zhang et al.'s method [31] and other variational models. Results showed the efficacy of our method.

Acknowledgments. The authors are grateful to the editor and referees for their valuable comments and suggestions that led to the improvement of this paper.

REFERENCES

[1] P. Alfeld, M. Neamtu and L. L. Schumaker, Fitting scattered data on sphere-like surfaces using spherical splines, *J. Comput. Appl. Math.*, **73** (1996), 5–43.
[2] M. Botsch, L. Kobbelt, M. Pauly, P. Alliez and B. Lévy, *Polygon Mesh Processing*, A. K. Peters, Ltd, 2010.
[3] J. F. Cai, S. Osher and Z. Shen, Split bregman methods and frame based image restoration, *Multiscale Model. Simul.: A SIAM Interdiscip. J.*, **8** (2009), 337–369.
[4] J. F. Cai and Z. Shen, Framelet based deconvolution, *J. Comput. Math.*, **28** (2010), 289–308.
[5] U. Clarenz, U. Diewald and M. Rumpf, Anisotropic geometric diffusion in surface processing, in *Proceedings of the Conference on Visualization 2000*, (2000), 397–405.
[6] M. Desbrun, M. Meyer, P. Schröder and A. H. Barr, Implicit fairing of arbitrary meshes using diffusion and curvature flow, in *Proceedings of SIGGRAPH 1999*, (1999), 317–324.
[7] M. Desbrun, M. Meyer, P. Schröder and A. H. Barr, Anisotropic feature-preserving denoising of height fields and bivariate data, in *Proceedings of the Graphics Interface 2000 Conference*, (2000), 145–152.
[8] B. Dong, Sparse representation on graphs by tight wavelet frames and applications. *Appl. Comput. Harmon. Anal.*, **42** (2017), 452–479.
[9] B. Dong, Q. T. Jiang, C. Q. Liu and Z. Shen, Multiscale representation of surfaces by tight wavelet frames with applications to denoising, *Appl. Comput. Harmon. Anal.*, **41** (2016), 561–589.
[10] B. Dong and Z. Shen, MRA-based wavelet frames and applications, *IAS/Park CityMathematics Series*, **19** (2010), 9–158.
[11] M. Elsey and S. Esedoglu, Analogue of the total variation denoising model in the context of geometry processing, *Multiscale Model. Simul.*, **7** (2009), 1549–1573.
[12] Z. T. Fan, H. Ji and Z. Shen, Dual Graminan analysis: Duality and unitary extension principle, *Math. Comp.*, **85** (2016), 239–270.
[13] S. Fleishman, I. Drori and D. Cohen-Or, Bilateral mesh denoising, *ACM Trans. Graph.*, **22** (2003), 950–953.
[14] Z. Gong, *Augmented Lagrangian Based Algorithms for Convex Optimization Problems with Non-separable ℓ_1-regularization*, Ph.D. thesis, National University of Singapore, 2013.
[15] Z. Gong, Z. Shen and K. Toh, Image restoration with mixed or unknown noises, *Multiscale Model. Simul.*, **12** (2014), 458–487.
[16] H. Hoppe, T. Derose, T. Duchamp, M. Halstead, H. Jin, J. Mcdonald, J. Schweitzer and W. Stuetzle, Piecewise smooth surface reconstruction, in *Proceedings of the 21st annual conference on Computer graphics and interactive techniques*, (1994), 295–302.
[17] T. Jones, F. Durand and M. Desbrun, Non-iterative, feature-preserving mesh smoothing, *ACM Trans. Graph.*, **22** (2003), 943–949.
[18] J. Li, Z. Shen, R. J. Yin and X. Q. Zhang, A reweighted ℓ^2 method for image restoration with poisson and mixed poisson-gaussian noise, *Inverse Probl. Imaging.*, **9** (2015), 875–894.
[19] S. Mallat, *A Wavelet Tour of Signal Processing: The Sparse Way*, Academic press, 2009.
[20] Y. Nesterov, A method of solving a convex programming problem with convergence rate $O(1/k^2)$, *Soviet Math. Dokl*, **27** (1983), 372–376.
[21] R. T. Rockafellar, Augmented Lagrangians and applications of the proximal point algorithm in convex programming, *Math. Oper. Res.*, **1** (1976), 97–116.
[22] A. Ron and Z. Shen, Affine systems in $L_2(\mathbb{R}^d)$: The analysis of the analysis operator, *J. Funct. Anal.*, **148** (1997), 408–447.
[23] L. I. Rudin, S. Osher and E. Fatemi, Nonlinear total variation based noise removal algorithms, *Phys. D*, **60** (1992), 259–268.

[24] R. B. Rusu, Z. C. Marton, N. Blodow, M. Dolha and M. Beetz, Towards 3D Point cloud based object maps for household environments, *Rob. Auton. Syst.*, **56** (2008), 927–941.
[25] Y. Shen, B. Han and E. Braverman, Removal of mixed gaussian and impulse noise using directional tensor product complex tight framelets, *J. Math. Imaging Vis.*, **54** (2016), 64–77.
[26] X. F. Sun, P. L. Rosin, R. R. Martin and F. C. Langbein, Fast and effective feature-preserving mesh denoising, *IEEE Trans. Vis. Comput. Graphics*, **13** (2007), 925–938.
[27] T. Tasdizen, R. Whitaker, P. Burchard and S. Osher, Geometric surface processing via normal maps, *ACM Trans. Graph.*, **22** (2003), 1012–1033.
[28] C. Wu, J. Zhang, Y. Duan and X. C. Tai, Augmented lagrangian method for total variation based image restoration and segmentation over triangulated surfaces, *J. Sci. Comput.*, **50** (2012), 145–166.
[29] M. Yan, Restoration of images corrupted by impulse noise and mixed gaussian impulse noise using blind inpainting, *SIAM J. Imaging Sci.*, **6** (2013), 1227–1245.
[30] J. Yang, D. Stahl and Z. Shen, An analysis of wavelet frame based scattered data reconstruction, *Appl. Comput. Harmon. Anal.*, **42** (2017), 480–507.
[31] H. Zhang, C. Wu, J. Zhang and J. Deng, Variational mesh denoising using total variation and piecewise constant function space, *IEEE Trans. Vis. Comput. Graphics*, **21** (2015), 873–886.

Received August 2016; revised May 2017.

E-mail address: jbyang@hhu.edu.cn
E-mail address: wangc0705@hhu.edu.cn